Organic Electronics 65 (2019) 412–418

Contents lists available at ScienceDirect

Organic Electronics

journal homepage: www.elsevier.com/locate/orgel

Stable Hall voltages in presence of dynamic quasi-continuum bands in poly (3,4-ethylene-dioxythiophene)

Philipp Stadler[a,*], Lucia N. Leonat[a,b], Reghu Menon[c], Halime Coskun[a], Sandrine van Frank[d], Christian Rankl[d], Markus C. Scharber[a]

[a] Institute of Physical Chemistry, Johannes Kepler University Linz, Altenberger Straße 69, 4040, Linz, Austria
[b] National Institute for Materials Physics, Atomistilor Str., No. 405A PO Box MG 7, 077125, Magurele, Romania
[c] Indian Institute of Science, Department of Physics, Bangalore, India
[d] Research Center for Non Destructive Testing GmbH, 4040, Linz, Austria

ARTICLE INFO

Keywords:
Hall-effect
Conducting polymers
Weak localization
Organic phase model
Electron coherence
PEDOT

ABSTRACT

Topological and thermal disorder complicate the mobility characterization in poly(3,4-ethylenedioxythiophene) systems and presently leaves the exact transport mechanisms not fully understood. Here we show that *ac*-Hall measured by lock-in amplifier is able to resolve the Hall voltage in semimetallic polymers between room temperature and 32 K. These results are evaluated using an organic random phase model. This accounts for the role of tail states and, particularly, for thermal disorder of molecular semiconductors. We report band mobilities up to 3.7 $cm^2 V^{-1} s^{-1}$ in semimetallic polymers occurring in delocalized bands that originate from significant electron coherence across the polymer chains.

1. Introduction

In crystalline semiconductors the Hall-effect represents the method to derive the charge carrier mobility. However, in disordered, emerging semiconductors it is rarely applied, because the band continuum becomes disrupted with the consequence of significantly decreased charge carrier mobilities and, hence, reduced Hall voltages [1–6]. These effects are amplified in molecular semiconductors, because on top of topological disorder, thermal disorder plays major role [7–15]. The related phonon-dynamics cause a significant stronger disorder screening of the Hall voltages as compared to inorganic systems and, subsequently, makes Hall characterization elaborate. For inorganic systems such as highly-doped silicon, there exist theoretical transport models that relate mainly the topological effects on the transverse Lorenz forces: we refer here to Friedman, who proposed such compensation in his random phase model (RPM) [1–4,16]. However, for disordered molecular semiconductors the phase model requires adaptions, in particular the relation of localization and doping. An organic phase model reconciling molecular dynamics had been suggested by *Yi* et al. [8]. It bases on the assumption that the transverse Lorentz forces are practically compensated by hopping carriers and that only the band carriers contribute to the Hall-effect. This leads to a significant reduced Hall voltage *i.e.* Hall voltage screening, which has to be considered in mobility calculation. The classic hypothesis of quasi-band continuum (coherent band-like transport) was here adapted for molecular systems to allow the extraction of mobilities in the presence of dynamic disorder. We concluded that at moderate disorder the residual band widths would be larger than the random disorder potentials fluctuations emerging from thermal and topological disorder. This would yield ultimately transport with persistent band contribution and stable Hall voltages (Fig. 1).

Our main assumption was that such situation is established in semimetallic conducting polymers - a class of molecular semiconductor, where the electrical conductivities are in the range of 1000 S cm^{-1}. These systems possess a metal-insulator transition at lower temperatures [17–26], so there exists evidence of a band contribution to the transport.

We demonstrate the characterization and evaluation of the screened Hall effect in commonplace, semimetallic poly(3,4-ethylene-dioxythiophenes) (PEDOTs) with the help of the organic phase model and as such we derive band mobilities from the Hall voltages. The study includes a complementary terahertz (THz) spectroscopy mobility characterization [27,28] for the system with the highest conductivity showing a similar mobility. We discuss the effect of long-range electron coherence among the polymer chains and the subsequent semimetallic transport properties (Anderson localization) with stable Hall voltages as result order from optimized solvent processing and post-processing treatments

* Corresponding author. Present: Linz Institute of Technology (LIT) and Institute of Physical Chemistry, Johannes Kepler University Linz, Altenberger Straße 69, 4040, Linz, Austria.
E-mail address: Philipp.Stadler@jku.at (P. Stadler).

https://doi.org/10.1016/j.orgel.2018.12.001
Received 1 June 2018; Received in revised form 26 November 2018; Accepted 2 December 2018
Available online 03 December 2018

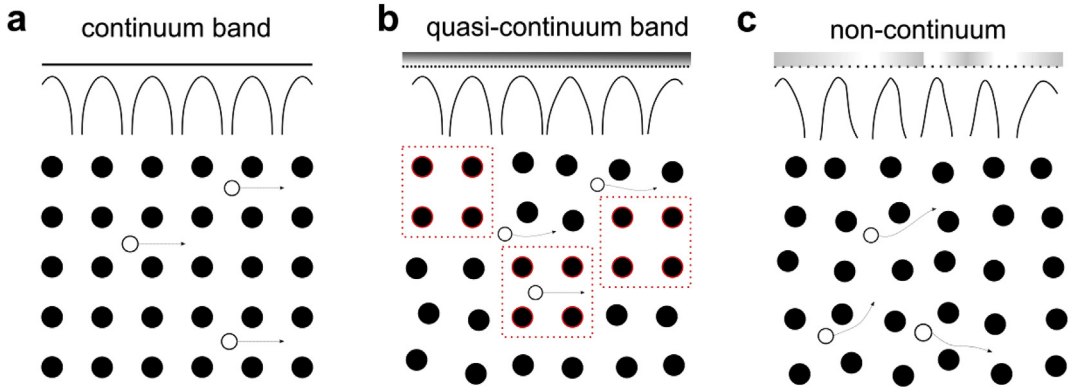

Fig. 1. (a) The change of the band structure upon increase of disorder leads to full disruption of the continuum as schematically proposed by (c). (b) Intermediate state of a quasi-band continuum is the existence of adjacently ordered domains inside a moderately disordered system.

[21–26,29–31].

Our Hall study includes three representative semimetallic PEDOT systems. In all these PEDOTs we are able to measure finite Hall-voltages. To probe these, we advanced the experimental setting using magnetic lock-in amplification (*i.e.* an *ac*-magnetic field B_{ac} combined with an electrical *dc* measurement, further denoted as *ac*-Hall). This technique expands the noise limit to 10^{-7} V in a van der Pauw Hall-specimen. Our experimental precision allowed us to measure consistent stable Hall voltages in the range of 10^{-6} V, which were then evaluated by the organic phase model between 32 and 300 K. In the best PEDOT, we calculate band mobilities of up to 3.7 $cm^2 V^{-1} s^{-1}$ [32–36] and these values are in agreement results from the contactless THz spectroscopy. We demonstrated that the hypothesis of quasi-band continuum can be utilized for the Hall effect in semimetallic polymers, where despite of the dynamic disorder, significant electron coherence resulted in stable Hall voltages and comparatively significant mobilities [37–40].

2. Results and discussion

As the diffusive band transport is significantly affected by dynamic disorder effects, the measurement of reduced Hall voltages (V_H) and its interpretation is often regarded as a challenging task. In this work we resolved the experimental and theoretical difficulties for the class of conducting polymers. We demonstrated that in semimetallic systems a consistent Hall voltage exists, which were evaluated by an organic phase model. We elucidated additive and acid-treated PEDOT-systems, which were applied as transparent electrodes and thermoelectric layers earlier. In general, latest advancements boosted the electrical conductivities of PEDOT-composites to metal-like regimes. These results relied on precise solvent processing and post-treatment steps and conductivities as high as 5000 S cm^{-1} and beyond have been achieved. Although these conductivity values are of impressive magnitude, the Hall-effect was not extensively studied [41–43].

We refer to processing strategies which utilized high boiling point polar co-solvents to obtain long-range order. Such additives were combined with spin-coating, blade-coating and printing and led typically to semimetallic transport. One common additive is dimethylsulfoxide (DMSO). DMSO-based formulations of PEDOT:PSS were matter of extensive studies, one of which is presented in the supplementary information (SI). In addition, we elucidated an alternative post-processing treatment with trifluoromethylsulfonic acid (TfOH). Exposure to the strong acid removes the polystyrenesulfonate anion (PSS^-) leading to the class of PSS-free PEDOT-systems (here subsequently called PEDOT:TfO with a conductivity of approx. 2000 S cm^{-1} and semimetallic transport behaviour). Both the DMSO and TfOH-treatments led to high electrical performance – ideal to conduct the combined transport and Hall-survey [44,45] (Table 1).

Table 1
PEDOT-systems for the Hall study covering state-of-the-art treatment strategies and conductivities.

	System	treatment	impact	Anion	σ_{300K}/ S cm^{-1}
1	PEDOT:PSS	10% DMSO	co-solvent additive	PSS^-	640
2	PEDOT:PSS*	5% DMSO	co-solvent additive	PSS^-	997
3	PEDOT:TfO	TfOH	solid-state, post-casting	TfO^-	1987

For the complementary temperature-dependent electrical conductivity σ(T) and Hall voltage V_H(T) we used 4-point probe and/or van der Pauw configurations between 300 K and 2 K (Fig. 2). As earlier reported we observed a transition regime between localization and delocalization (weak localization). The overlap was apparent at approximately 10 K ± 3 K, where the system is dominated either by temperature-activated Arrhenius-type transport (equation (1)) or by metal-like and rather *T*-independent transport (following Mott's theorem) [46]. We focussed the overlap regime at higher *T* and determine the activation energies E_A for each system from a log σ vs. T^{-1} plot (Table 2). The values reported here were in agreement with earlier findings. They correspond to the effective band width ($E_A \approx W_B$) of the quasi-band structure [16,46].

W_B can be used as estimate for the degree of disorder and the distribution between band and hopping carriers. The value also corresponds to the extent of a quasi-continuum *i.e.* the energy offset within the band between Fermi energy E_F and mobility edge E_C. (Fig. 2c and d).

$$\ln \frac{\sigma_T}{\sigma_{min}} = -\frac{E_c - E_F}{k_B} \cdot \frac{1}{T} \qquad \text{when} \quad W_B \cong E_c - E_F \tag{1}$$

Among the investigated systems, W_B was lowest in PEDOT:TfO at 0.76 meV (in agreement with the higher conductivities), while in PEDOT:PSS(*) it increases to 0.86 meV and 1.11 meV, respectively (Table 2). In a next step, we probed the probe the Hall voltage in parallel for all systems as function of temperature (Fig. 3). Therefore we patterned a PEDOT cloverleaf from a mastered substrate and process the polymer directly to a van der Pauw (vdP) specimen resulting in a symmetry factor close to unity. Across the edges we applied a 1 mA *dc*-current i_x constantly (note that all PEDOT-systems are electrically stable up to 10 mA under day-long high-current stress tests) (Fig. 3a). On top, a magnetic *ac*-field 0.625 T root mean square (RMS) amplitude (B_{ac}) was sinusoidally modulated at a frequency of 100 mHz to generate the *ac*-Hall voltage that was read out through a lock-in amplifier (Fig. 3b). The technique improves the signal-to-noise ratio and the noise limit of the setup through effective Faraday and misalignment compensation so that the Hall mobilities μ_H of down to 10^{-3} $cm^2 V^{-1} s^{-1}$ can be measured (Fig. 3c).

For example, we present the PEDOT:PSS* system (1) at 32 K: A Hall

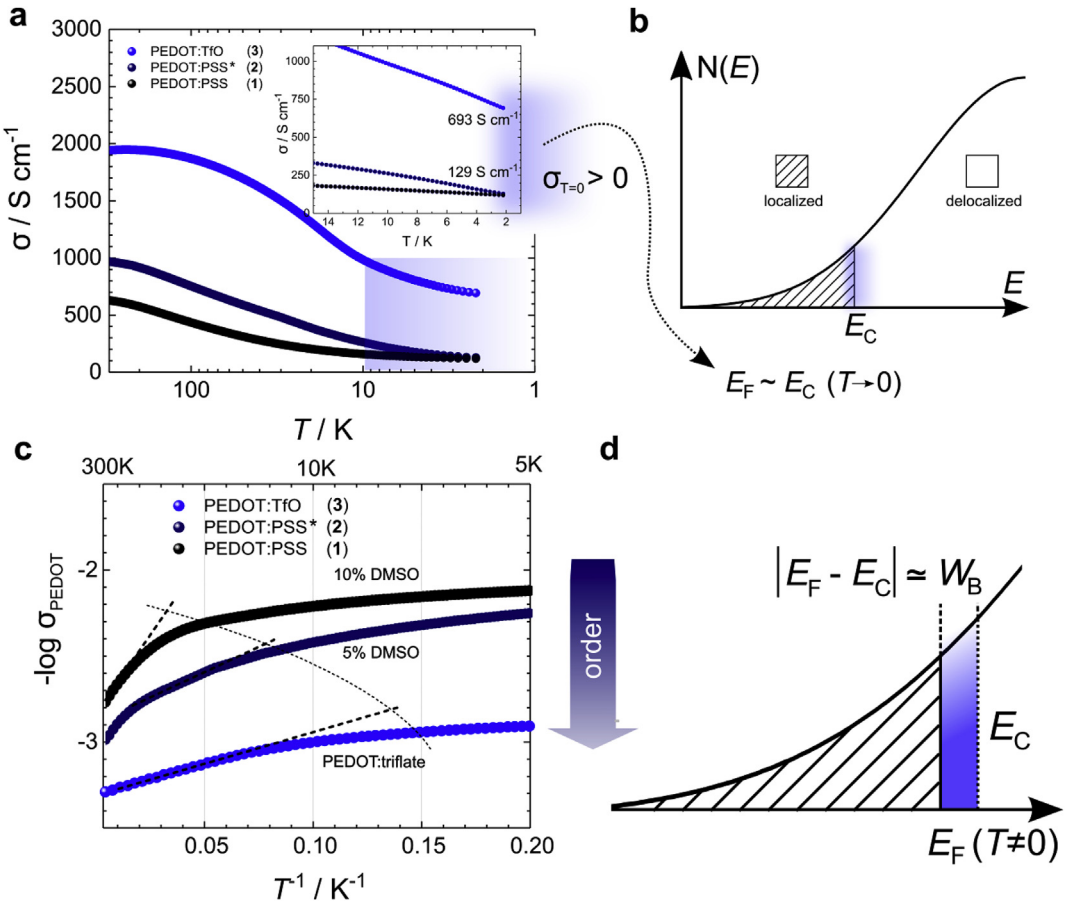

Fig. 2. Determination of band width W_B from σ –T plots (a) Semilog σ –T of various PEDOT-systems showing finite conductivity as T approaches 0 (inset: linear plot of σ –T below 10 K). (b) Schematic of the shallow transport regime at E_F close to E_C in PEDOT-systems. (c) Expanded plot for comparison: Note the slope (indicated as linear fits) at high-T are proportional to the band width W_B. (d) Schematic of band width $W_B \sim E_C$ - E_F in the vicinity of the metal-insulator transition regime (Anderson localization).

Table 2
Energies (band widths) as derived from log σ vs. T^{-1} plots (Fig. 2b).

System		slope/ K	W_B/ meV	σ_{300K}/ S cm^{-1}	σ_{2K}/ S cm^{-1}
1	PEDOT:PSS	12.9	1.11	640	120
2	PEDOT:PSS*	10.0	0.86	997	130
3	PEDOT:TfO	8.9	0.76	1987	690

voltage as large as $1.3 \cdot 10^{-6}$ V was generated at 1 mA *dc*-current and at modulated magnetic field with maximum amplitude at 0.91 T at 100 mHz. The Hall voltages increases linearly with increasing i_x between 1 and 10 mA (Fig. 3a).

The *ac*-Hall measurement was performed across all temperatures between 300 K and 32 K. Below 32 K, the *ac*-modulation has not been accessible because of Eddy current heating of the substrate holder (Fig. 4). All samples showed a Hall voltage range between $0.3 \cdot 10^{-6}$ V up to $6.0 \cdot 10^{-6}$ V at 1 mA. The absolute resistance of the specimen was in the range between 200 and 20 Ω. The sample thickness corresponded to typical dimensions used in applications ranging between 30 nm and 60 nm. The *ac*-modulation included a statistical evaluation – we reported a standard deviation for V_H at 1% for 100 repetitions. The measurement time expands to about 1 h per point with 100 repetitions at 100 mHz frequency.

From the data we derived the Hall constants R_H and the product of the Hall constant and conductivity *i.e.* the measured mobility μ (Table 3). The Hall parameters are comparable only the thickness is different. The $R_H(T)$ shows an inverse profile as compared to that of σ(T) (Fig. 4). This result reflects the ambiguity of the transport in polymers depicting the overlap of metallic and non-metallic transport mechanisms and the contribution of thermal-activation at higher *T*s. Consequently the product σR_H(T) is constant and its magnitude correlates to the electrical performances of the PEDOT-systems with PEDOT:TfO showing the highest (see Table 4).

The observations on $R_H(T)$ were in agreement with the organic phase model through (topological and thermal) disorder in molecular systems. Direct consequence is the comparatively low V_H and, subsequently, low R_H values (situated here at 10^{-4} cm^3 C^{-1}, as compared to approximately 10^{+2} in p-Si, from *ac*-Hall demonstrated in the **SI**). The product $\sigma R_H(T)$ *i.e.* the measured mobilities *i.e.* σR_H are far below the intrinsic band mobility, as suggested by the electrical conductivity values and their corresponding metal-like low-temperature behaviour.

Obviously, there exists a strong discrepancy between the *band* mobility μ_{band} and *hopping* mobility $\mu_{hopping}$ in the polymers as result of probing conditions and disorder *i.e.* thermal effects, anisotropy and hole-hole interaction. We utilized now the organic phase model to estimate the band mobility μ. Therefore we used the ratio β between $\mu_{hopping}$ and μ_{band}, as well as the factor γ as the distribution of delocalized carriers upon temperature with g as the degeneration factor and the activation energy E_A or band width W_B. In case of 3 dimensions g is equal to 6 (equation (2)). Such evaluations are also suggested in inorganic, disordered systems, where the μB product is significantly below unity (*e.g.* $1 \cdot 10^{-5}$ for the here studied PEDOTs at 0.625 T B_{ac} and measured μ around 0.1 and below) [47–49].

$$\mu \cdot B \ll 1 \quad \frac{\mu_{hopping}}{\mu_{band}} = \beta \ll 1 \quad \frac{n_{band}}{n_{total}} = 1 - g^{-1} \cdot e^{-\left(E_A/kT\right)} = \gamma \ll 1 \qquad (2)$$

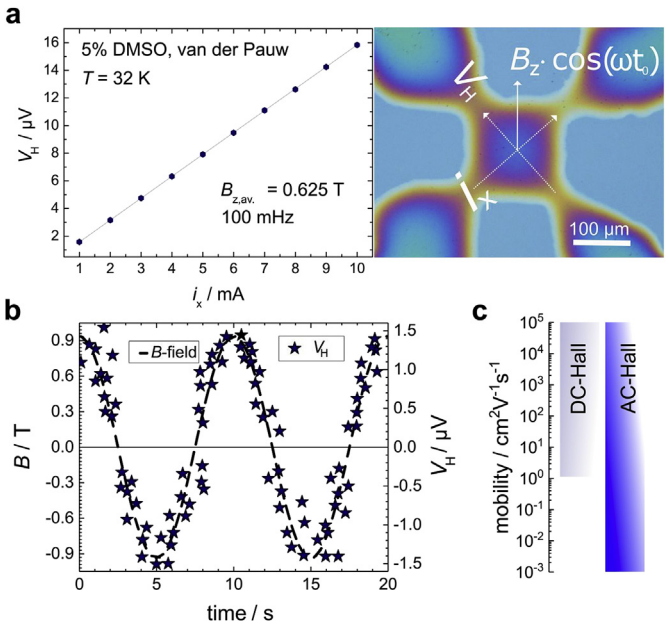

Fig. 3. *ac*-Hall detection (a) Average Hall-potential (i_x between 1 and 10 mA) of typical PEDOT:PSS (conductivity at 32 K is 500 S cm^{-1}) as derived from a simple van der Pauw geometry (picture). (b) 2 loops at 100 mHz of repeating magnetic *ac*-modulated Hall signal output (in µV) from sinusoidal applied magnetic field *B*. (c) Mobility expansion from *ac*-Hall diminishes misalignment potentials expanding the Hall mobility range to 10^{-3} cm^2 V^{-1} s^{-1}.

To compensate now the effect of Hall voltage screening, it was suggested by *Li* et al. [8] in their organic phase model that the band mobility μ_{band} can be estimated by inserting the correction factors β and γ: accordingly, only band carriers contribute to the Hall voltage, but they represent a minority in the Arrhenius regime above 10 K. We reconciled the disorder screening and the subsequent underestimation of the band mobility by assuming lower hopping than band mobility ($\beta << 1$) and, similarly, a low band contribution of the carriers (γ in the range of 10^{-4}, as calculated from equation (2)). This intermediate band contribution scenario led to a situation, where the band mobility was much higher than the measured Hall mobility μ in the weak *B*-field regime at moderate disorder, where the transverse electric fields E_y are low as compared to the longitudinal E_x (equation (3)).

$$\mu = \mu_{band} \cdot \frac{\gamma}{\gamma - \beta\gamma + \beta}\left(=\frac{E_y}{E_x B}\right) \quad n_{total} = n_{measured} \cdot \frac{(\gamma - \gamma\beta + \beta)^2}{\gamma} \tag{3}$$

For our case of semimetallic polymers we employed the intermediate hopping contribution regime assuming a weak band-like character and calculate $\gamma(T)$ using the band widths from the conductivity temperature profile ($W_B = E_A$) (equation (2)).

$$\gamma = (\gamma - \gamma\beta + \beta)^2 \quad \mu(T) = \mu_{band} \cdot \sqrt{\gamma(T)} \tag{4}$$

We use the re-formulated equation to derive β (equation (5)),

$$\beta^{-1} = 1 + \frac{1}{\sqrt{\gamma}} \tag{5}$$

and subsequently the corrected n_{total} and μ_{band} across the measured temperature regime (300–32 K). (Fig. 5). We show the organic phase model yields the volumetric carrier concentration n_{total} (Fig. 5a). The calculated μ_{band} shows the weak band-like temperature profile *i.e.* it decreases with temperature (Fig. 5b) and the band-character correlates with the magnitude of the conductivity *i.e.* most pronounced for PEDOT:TfO. We found that the organic phase model delivers reasonable values for the PEDOT-systems: The Hall voltage corresponds to a calculated n_{total} below the maximum doping ratio limited by the polymer's mass density, molar mass and maximum 1 dopant per monomers, $3.1 \cdot 10^{+21}$ cm^{-3} maximum). The profile of $n_f(T)$ indicates that at low temperatures the doping ratios saturate at the maximum limit. Hence, the transport is ultimately approaching the band regime. This is in agreement with earlier results at low temperatures in semimetallic PEDOT:TfO [20]. In order to confirm the band mobility, we included an alternative measurement of the transport parameters by Terahertz (THz) spectroscopy for PEDOT:TfO. The results yield slightly higher mobilities (3.1 cm^2 V^{-1} s^{-1}). The corresponding analysis and frequency-dependent conductivity is presented in the **SI**.

For PEDOT:TfO the maximum μ_c found is 3.7 cm^2 V^{-1} s^{-1}, whereas in PEDOT:PSS(*) μ_{band} are lower between 1.0 and 0.5 cm^2 V^{-1} s^{-1}, respectively. The temperature profiles for conductivity, mobility and carrier concentration suggest weak band contribution at higher temperatures, while at lower temperatures the band regime dominates. This follows the theory of weak localization *i.e.* there exists an overlap regimes between localized and delocalized transport and a transition regime around 10 K.

The magnitudes of μ_{band} are comparatively high in view of results on similar molecular semiconductors. Our results show that polymers possess a *systematic* degree of structural order. This had been reflected by their superior electrical performances and by our findings on the Hall-effect, which are in agreement with the literature discussing the

Table 3
Hall parameters at room temperature (300 K).

System		d_{film}/ nm	*(ac-)B*-field/ T	i_x/ A	R_H/ cm^3 C^{-1}
1	PEDOT:PSS	61	0.625	10^{-3}	$5.5 \cdot 10^{-5}$
2	PEDOT:PSS*	54	0.625	10^{-3}	$7.9 \cdot 10^{-5}$
3	PEDOT:TfO	30	0.625	10^{-3}	$1.0 \cdot 10^{-4}$

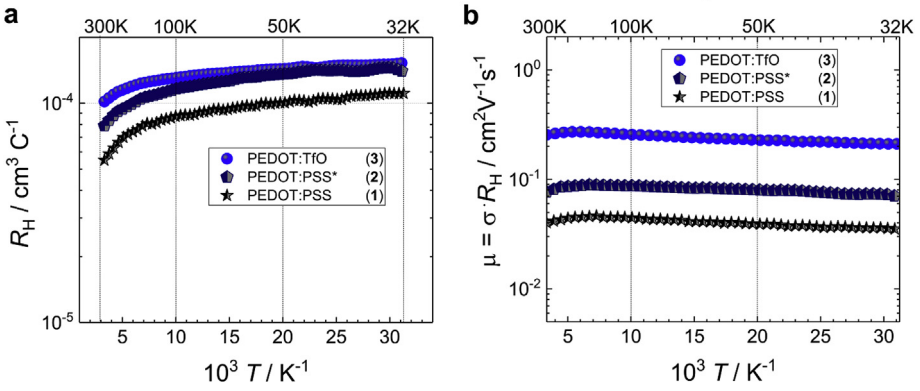

Fig. 4. (a) Experimental Hall-constant R_H vs. temperature reveals the quenched Hall voltage at the order of R_H at 10^{-4} cm^3 C^{-1} (*i.e.* the corresponding Hall voltage is 10^{-6} V). The R_H depends on the temperature reciprocal to the conductivity σ. (b) The measured mobility $\mu = \sigma R_H$ is thus constant.

Table 4
Hall parameters at room temperature (300 K).

System		μ_{band} at 300 K/ $cm^2 V^{-1} s^{-1}$	n_{total} at 300 K/ cm^{-3}	μ_{band} at 32 K/ $cm^2 V^{-1} s^{-1}$	n_{total} at 32 K/ cm^{-3}
1	PEDOT:PSS	0.5	$8.0 \cdot 10^{+20}$	0.15	$3.1 \cdot 10^{+21}$
2	PEDOT:PSS*	1.0	$4.3 \cdot 10^{+20}$	0.33	$2.0 \cdot 10^{+21}$
3	PEDOT:TfO	3.7	$2.3 \cdot 10^{+20}$	1.03	$1.3 \cdot 10^{+21}$

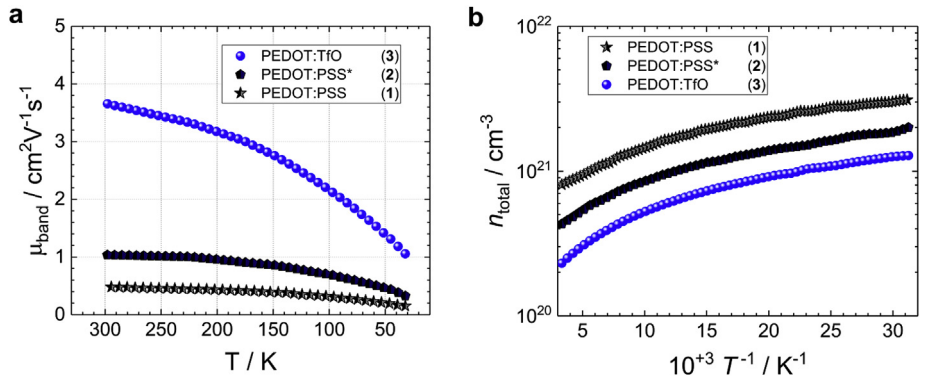

Fig. 5. Organic phase model applied to PEDOTs to evaluate the Hall-effect in the presence of dynamic disorder. (a) The band mobilities (μ_{band}) decrease with temperature, while in (b) the free carrier concentration increases at lower temperatures (less contribution from trapping, phonons).

extent of order in PEDOT-systems by electron coherence among the polymer chains [29].

3. Conclusion

The impact of disorder on the Hall-effect has frequently been discussed for organic semiconductors. Here, we explored the transport in semimetallic conducting polymers and apply an organic phase model described earlier. This regards the role of dynamic disorder on the experimentally observed Hall-voltage screening through strong hopping contribution. We observed a stable Hall voltage from semimetallic conducting polymers and we could utilize these experimental results to derive temperature-dependent band mobilities and carrier concentrations. The organic phase model yields comparatively high mobilities, in particular for the PEDOT:TfO system. This was in agreement with in parallel performed THz mobility characterization. We explained the magnitude of the charge carrier mobility by the electron coherence. Analogous conclusions have been reported in semimetallic polymers from magnetometric experiments. Our results can be adopted for related emerging and disordered semiconductors such as perovskites polymorphs or nanocrystalline solids and it shows a path to interpret the Hall-effect of conducting polymers.

4. Methods

4.1. ac-Hall specimen fabrication

To obtain the van der Pauw cloverleaf (Figs. 3a), 1 × 1 cm sapphire substrates were previously cleaned in water (and detergent), then rinsed thoroughly with distilled water and with isopropylic alcohol. After drying with nitrogen, the substrates were treated for 5 min in oxygen plasma. Using a shadow mask, we evaporated 50 nm of tetratetracontane (TTC, Sigma Aldrich) to define the four contact arms at the edge of the cloverleaf. Then the samples were exposed to an trichloro (1H,1H,2H,2H-perfluorooctyl)silane (FOS) rich atmosphere inside a Petri dish to cover the surface around the TTC layer (negative of the final structure). After few minutes, the samples were taken outside and TTC and excess fluoroalkylsilane was removed by washing with toluene and acetone to expose a FOS-free cloverleaf structure in the centre of the substrate. On these patterned substrates, different formulations of PEDOT:PSS (PH1000, Heraeus Inc., stock solution specific addition of DMSO, 5–10 $\%_{volume}$), were spun in two consecutive stages of 25 rounds per second (rps) (2s second ramp, 10s duration) and 100 rps (2 s ramp, 10 s duration) followed by thermal treatment in inert atmosphere at 120 °C for 10 min, resulting in layers with 50–70 nm thickness. The post-processing using TfOH is directly performed after spin-coating (exposure of with trifluoromethansulfonic acid, Sigma Aldrich 97%, 1:1 molar in water, 10 min plus washing with water, repeating 3 times). To assure proper contacts, 4 supporting gold electrode arms (140 nm) were evaporated to touch the cloverleaf-edges at $3.6 \cdot 10^{-6}$ mbar at a rate of 0.1–0.3 nm s^{-1}.

4.2. ac-Hall measurements

For *ac*-Hall the as-patterned thin films are bonded to the electrical setup and transferred to the cryogenic magneto-system. The samples are then left overnight in He-atmosphere at 300 K for drying. After that, the specimens were characterized using resistivity and *ac*-Hall characterization (in a LakeShore Hall Measurement System 8400 and Quantum Design DynaCool PPMS). We applied temperature loops starting from 2 K and scanned up to 300 K for the resistivity. The ac-Hall technique could be applied from 32 K up to 300 K. The magnetic field is swept between 0 and 0.91T (with a room mean square field B_{ac} of 0.625T) at 100 mHz. This leads to a dc-voltage for the resistivity and an ac-voltage for the Hall signal. We apply consistently 1 mA dc-current across the sample specimen using the van der Pauw geometry. These measurements are repeated at higher current up to 10 mA (current stressing). We exclude degradation effect from local heating. The film thickness is determined by DekTak (Bruker) in the probing space area after the cryogenic measurement cycles.

TEM measurements are performed using a grid substrate mounted on the sapphire substrate to imitate identical surrounding as for the transport measurements. PEDOT-systems are then cast as described above. We denote in the present resolution, we did not find changes in the structrure between PEDOT:PSS (10% DMSO treated) and PEDOT:PSS* (5% DMSO treated). Indeed we find changes in the structure between TfOH-treated and PEDOT:PSS*. All room temperature conductivity measurements and thickness measurements for the DMSO-treatment map have been recorded using a 4-probe setup for the conductivities and DekTak (Bruker) to measure the thickness values.

For the entire map, approximately 40 samples have been investigated.

4.3. Terahertz spectroscopy

Terahertz (THz) spectroscopy is a non-contact and non-destructive method that can locally follow carrier dynamics on timescales of pico- to nanoseconds. In THz spectroscopy the electric field is directly recorded and as such both the amplitude and phase are extracted. We measured a PEDOT:TfO film (thickness 262 nm) an insulating glass substrate and determined the complex-valued conductivity according to:

$$\sigma(\omega) = \left(\frac{1 + N_{sub}}{Z_0 d_{film}}\right)\left(\frac{E_{sub}(\omega)}{E_{samp}(\omega)} - 1\right)$$

where N_{sub} is the complex refractive index of the substrate, z_0 the free space impedance, d_{film} the thickness of the PEDOT:TfO, ω the radial frequency of the THz field and E_{sub} and E_{samp} the Fourier transforms of the THz electric field transmitted through the substrate and the sample, respectively [27].

The THz setup allowed us to estimate the average conductivity σ_{DC} (σ_{THz}) = 1582 S cm^{-1} between 0.1 and 1.1 THz, value which given the high plasma frequency and scattering rate (estimated at ω_P = 3.99.10 + 15 Hz and Γ = 9.1.10^{+14} Hz, respectively) corresponds to the DC conductivity [28]. This leads to a mobility of μ_{Thz} = 3.1 cm^2 V^{-1} s^{-1}.

Competing interest

The authors declare no competing interests.

Author contributions

P. S. designed and directed the study. P.S. contributed to all experiments. P.S. H.C. and L.N.L. designed the film growth process and carried out the experimental work and corresponding analytical measurements. Hall- and conductivity measurements were carried out by L.N.L. and P.S. S.V.F, H.C. and C.R. conducted the THz spectroscopy. P.S. and M.C.S. carried out the modelling and the relevant calculations. M.C.S., R.M. and P.S. analysed the data. P.S. wrote the manuscript. All authors commented on the paper.

Acknowledgements

P.S. and R.M. are grateful to OeAD Austria (WTZ, IN10/2015) for financial support. P.S. acknowledges the financial support of the Austrian Science Foundation (FWF I3822-N37, “Nachhaltige Katalyse”). The authors thank Dominik Farka and N. Serdar Sariciftci for fruitful discussions. This project was supported by the strategic economic- and research program "Innovative Upper Austria 2020" of the province of Upper Austria.

Appendix A. Supplementary data

Supplementary data to this article can be found online at https://doi.org/10.1016/j.orgel.2018.12.001.

References

[1] D. Emin, The sign of the Hall effect in hopping conduction, Philos. Mag. A 35 (1977) 1189–1198, https://doi.org/10.1080/14786437708232944.
[2] J.W. Orton, M.J. Powell, The Hall effect in polycrystalline and powdered semiconductors, Rep. Prog. Phys. 43 (1980) 1263 http://stacks.iop.org/0034-4885/43/i=11/a=001.
[3] L. Friedman, N.F. Mott, The Hall effect near the metal-insulator transition, J. Non-Cryst. Solids 7 (1972) 103–108, https://doi.org/10.1016/0022-3093(72)90021-X.
[4] L. Friedman, Hall conductivity of amorphous semiconductors in the random phase model, J. Non-Cryst. Solids 6 (1971) 329–341, https://doi.org/10.1016/0022-3093(71)90024-X.
[5] R. Kubo, Statistical-mechanical theory of irreversible processes. I. General theory and simple applications to magnetic and conduction problems, J. Phys. Soc. Japan. 12 (1957) 570–586, https://doi.org/10.1143/JPSJ.12.570.
[6] B. Lee, Y. Chen, D. Fu, H.T. Yi, K. Czelen, H. Najafov, V. Podzorov, Trap healing and ultralow-noise Hall effect at the surface of organic semiconductors, Nat. Mater. 12 (2013) 1125–1129, https://doi.org/10.1038/nmat3781.
[7] Y. Chen, H.T. Yi, V. Podzorov, High-resolution ac measurements of the Hall effect in organic field-effect transistors, Phys. Rev. Appl. 5 (2016) 034008, https://doi.org/10.1103/PhysRevApplied.5.034008.
[8] H.T. Yi, Y.N. Gartstein, V. Podzorov, Charge Carrier coherence and Hall effect in organic semiconductors, Sci. Rep. 6 (2016) 23650, https://doi.org/10.1038/srep23650.
[9] R. Fujimoto, S. Watanabe, Y. Yamashita, J. Tsurumi, H. Matsui, T. Kushida, C. Mitsui, H.T. Yi, V. Podzorov, J. Takeya, Control of molecular doping in conjugated polymers by thermal annealing, Org. Electron. 47 (2017) 139–146, https://doi.org/10.1016/j.orgel.2017.05.019.
[10] J. Takeya, K. Tsukagoshi, Y. Aoyagi, T. Takenobu, Y. Iwasa, Hall effect of quasi-hole gas in organic single-crystal transistors, Jpn. J. Appl. Phys. 44 (2005) L1393–L1396, https://doi.org/10.1143/JJAP.44.L1393.
[11] N. Karl, Charge Carrier transport in organic semiconductors, Synth. Met. 133–134 (2003) 649–657, https://doi.org/10.1016/S0379-6779(02)00398-3.
[12] K. Imaeda, Y. Yamashita, Y. Li, T. Mori, H. Inokuchi, M. Sano, Hall-effect observation in the new organic semiconductor bis(1,2,5-thiadiazolo)-p-quinobis(1,3-dithiole)(BTQBT), J. Mater. Chem. 2 (1992) 115, https://doi.org/10.1039/jm9920200115.
[13] J. Takeya, J. Kato, K. Hara, M. Yamagishi, R. Hirahara, K. Yamada, Y. Nakazawa, S. Ikehata, K. Tsukagoshi, Y. Aoyagi, T. Takenobu, Y. Iwasa, In-Crystal and surface charge transport of electric-field-induced carriers in organic single-crystal semiconductors, Phys. Rev. Lett. 98 (2007) 196804, https://doi.org/10.1103/PhysRevLett.98.196804.
[14] J.-F. Chang, T. Sakanoue, Y. Olivier, T. Uemura, M.-B. Dufourg-Madec, S.G. Yeates, J. Cornil, J. Takeya, A. Troisi, H. Sirringhaus, Hall-effect measurements probing the degree of charge-Carrier delocalization in solution-processed crystalline molecular semiconductors, Phys. Rev. Lett. 107 (2011) 066601, https://doi.org/10.1103/PhysRevLett.107.066601.
[15] V. Podzorov, E. Menard, J.A. Rogers, M.E. Gershenson, Hall effect in the accumulation layers on the surface of organic semiconductors, Phys. Rev. Lett. 95 (2005) 226601, https://doi.org/10.1103/PhysRevLett.95.226601.
[16] N.F. Mott, Metal-insulator Transitions, Taylor & Francis LTD, 1974.
[17] C. Cobet, J. Gasiorowski, D. Farka, P. Stadler, Polarons in conjugated polymers, in: K.-J. Hinrichs, Eichhorn Karsten (Eds.), Ellipsom. Funct. Org. Surfaces Film, 2018, pp. 355–387, , https://doi.org/10.1007/978-3-319-75895-4_16.
[18] F. Dominik, A.O.F. Jones, R. Menon, N.S. Sariciftci, P. Stadler, Metallic conductivity beyond the Mott minimum in PEDOT: sulphate at low temperatures, Synth. Met. 240 (2018) 59–66, https://doi.org/10.1016/j.synthmet.2018.03.015.
[19] D. Farka, H. Coskun, P. Bauer, D. Roth, B. Bruckner, P. Klapetek, N.S. Sariciftci, P. Stadler, Increase in electron scattering length in PEDOT:PSS by a triflic acid post-processing, Monatshefte Für Chemie - Chem. Mon. 148 (2017) 871–877, https://doi.org/10.1007/s00706-017-1973-1.
[20] D. Farka, H. Coskun, J. Gasiorowski, C. Cobet, K. Hingerl, L.M. Uiberlacker, S. Hild, T. Greunz, D. Stifter, N.S. Sariciftci, R. Menon, W. Schoefberger, C.C. Mardare, A.W. Hassel, C. Schwarzinger, M.C. Scharber, P. Stadler, Anderson-localization and the mott-ioffe-regel limit in glassy-metallic PEDOT, Adv. Electron. Mater (2017) 1700050, https://doi.org/10.1002/aelm.201700050.
[21] P. Stadler, D. Farka, H. Coskun, E.D. Głowacki, C. Yumusak, L.M. Uiberlacker, S. Hild, L.N. Leonat, M.C. Scharber, P. Klapetek, R. Menon, N.S. Sariciftci, Local order drives the metallic state in PEDOT:PSS, J. Mater. Chem. C. 4 (2016) 6982–6987, https://doi.org/10.1039/C6TC02129H.
[22] S.D. Kang, G.J. Snyder, Charge-transport model for conducting polymers, Nat. Mater. 16 (2017) 252–257, https://doi.org/10.1038/nmat4784.
[23] A. Hamidi-Sakr, L. Biniek, J.-L. Bantignies, D. Maurin, L. Herrmann, N. Leclerc, P. Lévêque, V. Vijayakumar, N. Zimmermann, M. Brinkmann, A versatile method to fabricate highly in-plane aligned conducting polymer films with anisotropic charge transport and thermoelectric properties: the key role of alkyl side chain layers on the doping mechanism, Adv. Funct. Mater. 27 (2017) 1700173, https://doi.org/10.1002/adfm.201700173.
[24] M.N. Gueye, A. Carella, N. Massonnet, E. Yvenou, S. Brenet, J. Faure-Vincent, S. Pouget, F. Rieutord, H. Okuno, A. Benayad, R. Demadrille, J.-P. Simonato, Structure and dopant engineering in PEDOT thin films: practical tools for a dramatic conductivity enhancement, Chem. Mater. 28 (2016) 3462–3468, https://doi.org/10.1021/acs.chemmater.6b01035.
[25] J. Rivnay, S. Inal, B.A. Collins, M. Sessolo, E. Stavrinidou, X. Strakosas, C. Tassone, D.M. Delongchamp, G.G. Malliaras, Structural control of mixed ionic and electronic transport in conducting polymers, Nat. Commun. 7 (2016) 11287, https://doi.org/10.1038/ncomms11287.
[26] B.J. Worfolk, S.C. Andrews, S. Park, J. Reinspach, N. Liu, M.F. Toney, S.C.B. Mannsfeld, Z. Bao, Ultrahigh electrical conductivity in solution-sheared polymeric transparent films, Proc. Natl. Acad. Sci. Unit. States Am. 112 (2015) 14138–14143, https://doi.org/10.1073/pnas.1509958112.
[27] B.G. Alberding, P.A. DeSario, C.R. So, A.D. Dunkelberger, D.R. Rolison, J.C. Owrutsky, E.J. Heilweil, Static and time-resolved terahertz measurements of photoconductivity in solution-deposited ruthenium dioxide nanofilms, J. Phys. Chem. C 121 (2017) 4037–4044, https://doi.org/10.1021/acs.jpcc.6b12382.
[28] R. Ulbricht, E. Hendry, J. Shan, T.F. Heinz, M. Bonn, Carrier dynamics in semiconductors studied with time-resolved terahertz spectroscopy, Rev. Mod. Phys. 83

(2011) 543–586, https://doi.org/10.1103/RevModPhys.83.543.
[29] K. Kang, S. Watanabe, K. Broch, A. Sepe, A. Brown, I. Nasrallah, M. Nikolka, Z. Fei, M. Heeney, D. Matsumoto, K. Marumoto, H. Tanaka, S. Kuroda, H. Sirringhaus, 2D coherent charge transport in highly ordered conducting polymers doped by solid state diffusion, Nat. Mater. 15 (2016) 896–902, https://doi.org/10.1038/nmat4634.
[30] T.-R. Chou, S.-H. Chen, Y.-T. Chiang, Y.-T. Lin, C.-Y. Chao, Highly conductive PEDOT:PSS films by post-treatment with dimethyl sulfoxide for ITO-free liquid crystal display, J. Mater. Chem. C. 3 (2015) 3760–3766, https://doi.org/10.1039/C5TC00276A.
[31] A. Ugur, F. Katmis, M. Li, L. Wu, Y. Zhu, K.K. Varanasi, K.K. Gleason, Low-Dimensional conduction mechanisms in highly conductive and transparent conjugated polymers, Adv. Mater. 27 (2015) 4604–4610, https://doi.org/10.1002/adma.201502340.
[32] O.J. Sandberg, M. Nyman, S. Dahlström, S. Sandén, B. Törngren, J.-H. Smått, R. Österbacka, On the validity of MIS-CELIV for mobility determination in organic thin-film devices, Appl. Phys. Lett. 110 (2017) 153504, https://doi.org/10.1063/1.4980101.
[33] O.J. Sandberg, Effect of the depletion layer capacitance on the mobility determination using transient current extraction of doping-induced charge carriers, J. Photon. Energy 8 (2018) 1, https://doi.org/10.1117/1.JPE.8.032208.
[34] M. Nyman, O.J. Sandberg, S. Dahlström, D. Spoltore, C. Körner, Y. Zhang, S. Barlow, S.R. Marder, K. Leo, K. Vandewal, R. Österbacka, Doping-induced Carrier profiles in organic semiconductors determined from capacitive extraction-current transients, Sci. Rep. 7 (2017) 5397, https://doi.org/10.1038/s41598-017-05499-3.
[35] Y. Du, X. Cui, L. Li, H. Tian, W.-X. Yu, Z.-X. Zhou, Dielectric properties of DMSO-doped-PEDOT:PSS at THz frequencies, Phys. Status Solidi 255 (2018) 1700547, https://doi.org/10.1002/pssb.201700547.
[36] M. Yamashita, C. Otani, H. Okuzaki, M. Shimizu, Nondestructive measurement of Carrier mobility in conductive polymer PEDOT:PSS using Terahertz and infrared spectroscopy, XXXth URSI Gen. Assem. Sci. Symp. IEEE, 2011, pp. 1–4, , https://doi.org/10.1109/URSIGASS.2011.6050616 2011.
[37] G. Bergmann, Weak localization in thin films, Phys. Rep. 107 (1984) 1–58, https://doi.org/10.1016/0370-1573(84)90103-0.
[38] P.A. Lee, T.V. Ramakrishnan, Disordered electronic systems, Rev. Mod. Phys. 57 (1985) 287–337, https://doi.org/10.1103/RevModPhys.57.287.
[39] V. D'Innocenzo, A. Luzio, H. Abdalla, S. Fabiano, M.A. Loi, D. Natali, A. Petrozza, M. Kemerink, M. Caironi, Two-dimensional charge transport in molecularly ordered polymer field-effect transistors, J. Mater. Chem. C. 4 (2016) 11135–11142, https://doi.org/10.1039/C6TC03897B.
[40] Y. Chen, H.T. Yi, X. Wu, R. Haroldson, Y.N. Gartstein, Y.I. Rodionov, K.S. Tikhonov, A. Zakhidov, X.-Y. Zhu, V. Podzorov, Extended Carrier lifetimes and diffusion in hybrid perovskites revealed by Hall effect and photoconductivity measurements, Nat. Commun. 7 (2016) 12253, https://doi.org/10.1038/ncomms12253.
[41] E. Helgren, K. Penney, M. Diefenbach, M. Longnickel, M. Wainwright, E. Walker, S. Al-Azzawi, H. Erhahon, J. Singley, Electrodynamics of the conducting polymer polyaniline on the insulating side of the metal-insulator transition, Phys. Rev. B 95 (2017) 125202, https://doi.org/10.1103/PhysRevB.95.125202.
[42] E. Jin Bae, Y. Hun Kang, K.-S. Jang, S. Yun Cho, Enhancement of thermoelectric properties of PEDOT:PSS and tellurium-PEDOT:PSS hybrid composites by simple chemical treatment, Sci. Rep. 6 (2016) 18805, https://doi.org/10.1038/srep18805.
[43] A. Malti, J. Edberg, H. Granberg, Z.U. Khan, J.W. Andreasen, X. Liu, D. Zhao, H. Zhang, Y. Yao, J.W. Brill, I. Engquist, M. Fahlman, L. Wågberg, X. Crispin, M. Berggren, An organic mixed ion-electron conductor for power electronics, Adv. Sci. 3 (2016), https://doi.org/10.1002/advs.201500305 n/a-n/a.
[44] N. Massonnet, A. Carella, A. de Geyer, J. Faure-Vincent, J.-P. Simonato, Metallic behaviour of acid doped highly conductive polymers, Chem. Sci. 6 (2015) 412–417, https://doi.org/10.1039/C4SC02463J.
[45] N. Kim, S. Kee, S.H. Lee, B.H. Lee, Y.H. Kahng, Y.-R. Jo, B.-J. Kim, K. Lee, Highly conductive PEDOT:PSS nanofibrils induced by solution-processed crystallization, Adv. Mater. 26 (2014) 2268–2272, https://doi.org/10.1002/adma.201304611.
[46] N.F. Mott, Conduction in non-crystalline systems IX. the minimum metallic conductivity, Philos. Mag. A 26 (1972) 1015–1026, https://doi.org/10.1080/14786437208226973.
[47] W.C. Mitchel, P.M. Hemenger, Temperature dependence of the Hall factor and the conductivity mobility in p -type silicon, J. Appl. Phys. 53 (1982) 6880–6884, https://doi.org/10.1063/1.330028.
[48] F. Szmulowicz, Calculation of the mobility and the Hall factor for doped p -type silicon, Phys. Rev. B 34 (1986) 4031–4047, https://doi.org/10.1103/PhysRevB.34.4031.
[49] J.F. Lin, S.S. Li, L.C. Linares, K.W. Teng, Theoretical analysis of hall factor and hall mobility in p-type silicon, Solid State Electron. 24 (1981) 827–833, https://doi.org/10.1016/0038-1101(81)90098-8.